❏   1210

Proposed robust ADRC control of a DFIG used in wind power production

Abdeslam Jabal Laafou[1], Abdessalam Ait Madi[1], Youssef Moumani[1], Adnane Addaim[2]
[1]Advanced Systems Engineering Laboratory, National School of Applied Sciences, Ibn Tofail University, Kenitra, Morocco
[2]Mohammadia School of Engineers, Mohamed V University Rabat, Rabat, Morocco

Article Info	ABSTRACT
	This work presents the control of the double fed induction generator (DFIG) used in the wind conversion system (WCS). The studied model is based on the control of the two converters grid side converter (GSC) and rotor side converter (RSC), in order to extract the maximum of power and also to keep the direct current (DC) bus voltage constant. The control strategy used here is based on linear active disturbance rejection control (LADRC) controllers. These are known, in the field of control systems, by their performance and robustness and allow a very good rejection of disturbances which can affect the wind system. In addition, this kind of controllers could help to meet the requirements of robustness against the variations of the parameters of the system and the uncertainties of its mathematical model. To validate the effectiveness of the proposed control, the system was modeled and tested by numerical simulation using MATLAB/Simulink software. The results carried out are discussed and analyzed in terms of references tracking, robustness and disturbance rejection. The results obtained have shown shown that the proposed control is promising and useful.

Corresponding Author:

Abdeslam Jabal Laafou
Advanced Systems Engineering Laboratory, National School of Applied Sciences, Ibn Tofail University
Avenida de L'Université, Kenitra, Morocco
Email: abdeslam.jaballaafou@uit.ac.ma

1. INTRODUCTION

In Morocco, the production of renewable energies is growing faster than that of fossil fuels. This dynamic should continue in the future thanks to the significant national and international investments which will allow the country to gradually free itself from its energy dependence both in terms of its imports of hydrocarbons and electricity imported from abroad. As part of Moroccan energy transition strategy, wind energy is recommended in many scenarios to achieve the ambitious objectives set up, compared, economically and technologically, to other sectors of electricity production of renewable origin [1], [2].

In the literature, to control the active and reactive powers of the double fed induction generator (DFIG), the authors [3], [4] have respectively proposed the use of direct power control (DPC) and oriented stator flux vector control. Active and reactive power control is obtained with a controller called rotor current regulator or by modified direct power control (MDPC) [5]. However, the wind conversion system (WCS) is a complex system with non-linearities, multiple variables, and system parameter disturbances caused by the external environment. These problems should be taken into account to meet the challenge to obtain an accurate mathematical model [6]. Therefore, designing more detailed and effective control methods to solve these problems of different disturbances affecting the system is of great importance for the reliable operation of the WCS and also for extracting the maximum power from the wind turbine. Currently, many researches have been presented [3], [4] using proportional integral (PI) regulators and backstepping control [6] to

control rotor currents. But the problem is that its last two regulators are sensitive to the variation of the internal parameters of DFIG. Some authors have looked for other power control options for DFIG using model predictive control [7], sliding mode control [8], [9] or feedback linearization control [10].

The control strategies mentioned previously used for the control of the DFIG requires the knowledge of the mathematical model of the system, the uncertainty due to the knowledge of the parameters of the system can degrade the performances of the system [11]. To solve this problem a robust and powerful control method called linear active disturbance rejection control (LADRC) is involved. This last one is based on the estimation and real-time compensation of internal and external disturbances, which can affect the system [12], [13].

The LADRC control strategy is based on the linear extended state observer (LESO) which constitutes its core and allows estimate and cancel the various external and internal disturbances of the system in real time [14]. This observer has the advantage that it does not require complete knowledge and exact system to be controlled. Furthermore, it allows to reduce the time to establish a detailed model of the studied system.

In this present paper, the modeling strategy of DFIG is decribed; turbine, grid side converter (GSC), and filter, and then a robust control ADRC is applied to the control of the rotor side converter (RSC) and GSC. The test of the behavior of the system is highlighted using matlab/simulink software. Finally the last section concludes this work.

2. RESEARCH METHOD

2.1. Wind conversion system modeling

The Figure 1 as shown in represent the different blocks of WCS. Actually, three-bladed horizontal axis wind turbine structures are the most widely used in the medium and large power wind turbine industry. These structures are based on the DFIG, and are equipped with two back-to-back type converters; RSC and GSC, the latter are controlled independently of one of the other. A capacitor is placed between the two converters to stabilize the direct voltage. This topology allows the converter to extract approximately 30% of the total power produced [14], [15].
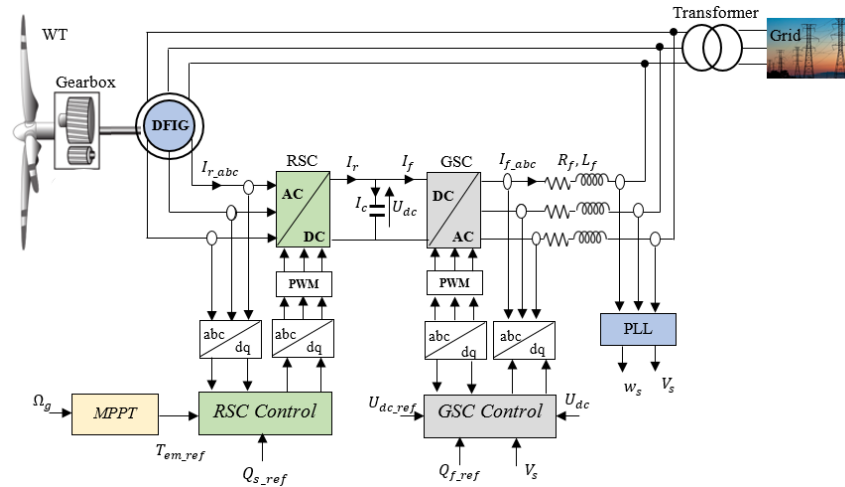

Figure 1. Block diagram of WCS based on DFIG

2.1.1. Wind turbine model

The function of the turbine is to convert the kinetic energy of the wind into mechanical energy of rotation. The extractable power available from the wind turbine (WT) is defined by (1).

$$P_{aer} = C_p \cdot Pv = C_p \cdot \frac{\rho.S.V^3}{2} \tag{1}$$

Where V is wind speed, ρ is the air density and $S = \pi R^2$ is the area swept by the turbine. The power coefficient Cp expression is defined by (2) [13], [16].

$$C_p(\lambda, \beta) = 0.5872 \left(\frac{116}{A} - 0.4\beta - 5 \right) e^{\frac{-21}{A}} + 0.0085\lambda \tag{2}$$

With:

$$\frac{1}{A} = \frac{1}{\lambda + 0.08\beta} - \frac{0.035}{1+\beta^3} \tag{3}$$

Where $C_p(\lambda, \beta)$ is the power coefficient, λ the speed ratio, and β the pitch angle. The gearbox ensures the connection between the turbine shaft to the generator shaft, its role is to adapt the speed between the turbine and the generator. The gearbox is modeled by a speed gain corresponding to the multiplication ratio given by the (4).

$$G = \frac{\Omega_g}{\Omega_{turbine}} \tag{4}$$

In order to establish the evolution of the mechanical speed from the total torque applied to the rotor of the generator, the fundamental (5) of dynamics is applied [14].

$$J\frac{d\Omega_g}{dt} = T_g - T_{em} - f_v\Omega_g \tag{5}$$

Where f_v is the viscous friction coefficient and J is total moment of inertia. The technique of extracting the maximum of the power consists in maintain the speed ratio λ at its optimal value λ_opt which make the power coefficient to its maximum value cpmax [14]-[16], Figure 2 as shown in represent the block diagram of the turbine with maximum power point tracker (MPPT).

Figure 2. Block diagram of the turbine with MPPT

2.1.2. Double fed induction generator model
The dynamic model in a $d - q$ reference frame of DFIG is writen by electrical (6) as shown in [15], [17].

$$\begin{cases} V_{sd} = R_s i_{sd} + \frac{d\phi_{sd}}{dt} - \omega_s\phi_{sq} \\ V_{sq} = R_s i_{sq} + \frac{d\phi_{sq}}{dt} + \omega_s\phi_{sd} \\ V_{rd} = R_r i_{rd} + \frac{d\phi_{rd}}{dt} - \omega_r\phi_{rq} \\ V_{rq} = R_r i_{rq} + \frac{d\phi_{rq}}{dt} + \omega_r\phi_{rd} \end{cases} \tag{6}$$

The electromagnetic torque T_{em} is illustrated by (7).

$$T_{em} = \frac{3}{2}p\frac{L_m}{L_s}(\phi_{sq}i_{rd} - \phi_{sd}i_{rq}) \tag{7}$$

To simplify the studied model, an orientation of the stator flux ψ along the d-axis is involved ($\phi_{sd} = \phi_s$, $\phi_{sq} = 0$), also stator resistance R_s is neglected [18], [19]. The DFIG stator voltages equations become (8).

$$\begin{cases} V_{sd} = R_s i_{sd} + \frac{d\phi_{sd}}{dt} = 0 \\ V_{sq} = \omega_s\phi_s \end{cases} \tag{8}$$

Active and reactive stator powers are expressed by (9).

$$\begin{cases} P_s = -\frac{3}{2}\frac{V_s L_m}{L_s} i_{rq} \\ Q_s = \frac{3}{2}(\frac{V_s \phi_s}{L_s} - \frac{V_s L_m}{L_s} i_{rd}) \end{cases} \tag{9}$$

Electromagnetic torque is given by (10).

$$T_{em} = -\frac{3}{2} p \frac{L_m}{L_s} \phi_s i_{rq} \tag{10}$$

2.2. Double fed induction generator control
2.2.1. Linear active disturbance rejection control model

The LADRC control makes it possible to compensate for all real disturbances and model uncertainties of the system with the help of an LESO which is the heart of this control strategy [20], [21]. To illustrate the principle of the LADRC, a first order system with single input u and single-output y is considered as described by (11).

$$\frac{dy(t)}{dt} = f(y, d, t) + b_0. u(t) \tag{11}$$

Where $f(y, d, t)$ represents the dynamic of the model and the total disturbances (internal and external) of the system and b_0 is the known part of the system. The representation in state variables of the system described by (11) is given as shown in (12) [20]–[22].

$$\begin{cases} \dot{x}_1 = x_2 + b_0. u \\ \dot{x}_2 = \dot{f} \\ y = x_1 \end{cases} \tag{12}$$

In matrix form:

$$\begin{cases} \begin{pmatrix} \dot{x}_1 \\ \dot{x}_2 \end{pmatrix} = \begin{pmatrix} 0 & 1 \\ 0 & 0 \end{pmatrix} \begin{pmatrix} x_1 \\ x_2 \end{pmatrix} + \begin{pmatrix} b_0 \\ 0 \end{pmatrix} u + \begin{pmatrix} 0 \\ 1 \end{pmatrix} \dot{f} \\ y = (1 \quad 0) \begin{pmatrix} x_1 \\ x_2 \end{pmatrix} \end{cases} \tag{13}$$

The first order LESO is illustrated in Figure 3, therefore the corresponding observer is presented by the (14).

$$\begin{cases} \begin{pmatrix} \dot{\hat{x}}_1 \\ \dot{\hat{x}}_2 \end{pmatrix} = \begin{pmatrix} -\beta_{01} & 1 \\ -\beta_{02} & 0 \end{pmatrix} \begin{pmatrix} \hat{x}_1 \\ \hat{x}_2 \end{pmatrix} + \begin{pmatrix} b_0 \\ 0 \end{pmatrix} u + Ly \\ \hat{y} = (1 \quad 0) \begin{pmatrix} \hat{x}_1 \\ \hat{x}_2 \end{pmatrix} \end{cases} \tag{14}$$

Where $\hat{y}$ is the estimated output, and L is the observer gain vector. For systems of n order, the general expression of the gains of the ESO observer are expressed by (15) [17].

$$\beta_{0i} = \frac{(n+1)!}{(n+1-i)!i!} \omega_o^i \tag{15}$$

Where $i = 1, 2, \cdots, n + 1$ and n is the system ordr, and ω_0 denotes the observer's cut-off pulse. According to relation (15), the gains of the ESO for the 1st order system is expressed by (16).

$$L = [\beta_{01} \quad \beta_{02}]^T = [2\omega_0 \quad \omega_0^2]^T \tag{16}$$

It should be noted that a large pulsation makes it possible to have a good estimation of the states, however this risks increasing the sensitivity to noise. It can be determined as a function of the poles of the closed-loop system [23]. Figure 3 illustrates the block diagram of the first-order LESO observer.

The estimated variables $\hat{x}_1 \rightarrow \hat{y}$ and $\hat{x}_2 \rightarrow \hat{f}$ are used to compensate the effect of all disturbances by applying the following control law, given by the (17).

$$u = \frac{u_0 - \hat{f}}{b_0} \tag{17}$$
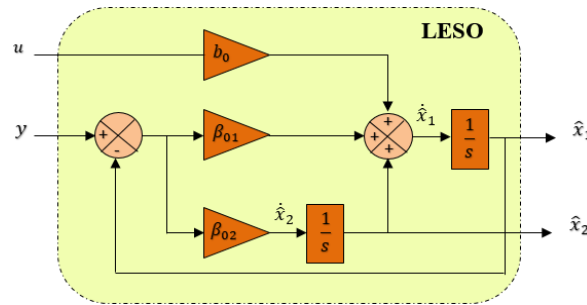
Where:

$$u_0 = k_c(r - \hat{y}) \tag{18}$$

Figure 3. First order LESO

Substituting (17) and (18) into (11) we get:

$$\dot{y} = f + b_0 . \frac{u_0 - \hat{f}}{b_0} = f - \hat{f} + k_c(r - \hat{y}) \tag{19}$$

If $f \approx \hat{f}$ and $\hat{y} \approx y$ we obtain:

$$\dot{y} = u_0 = k_c(r - y) \tag{20}$$

Hence the following differential (21).

$$\frac{1}{k_c}\dot{y} + y = r \tag{21}$$

We then obtain a closed-loop behavior of a first-order system having the pole: $-k_c$. The controller gain $-k_c$ is chosen such that $k_c = \omega_c = \frac{4}{\tau_r}$ where τ_r is the response time of the closed-loop system, ω_c is the closed loop natural frequency and r is the reference signal. The dynamics of the observer must be fast compared to that of the controller. Therefore, the poles of the observer are placed to the left of the poles of the closed-loop system. Generally, ω_0 is chosen such that $\omega_0 = (3 \sim 10)\omega_c$ [23], [24]. Figure 4 show the block diagram of the first-order LADRC.
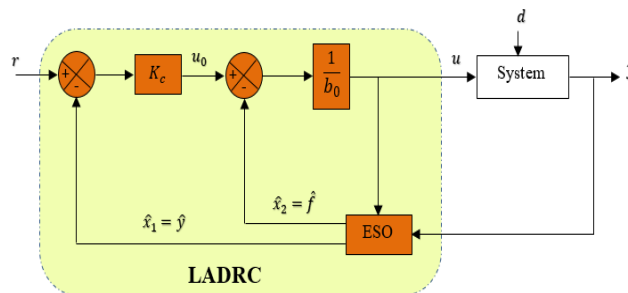
Figure 4. Block diagram of first order LADRC

2.2.2. Linear active disturbance rejection control for rotor side converter
        The simplified model of DFIG with stator field oriented shows that both direct and quadrature components of rotor current can be independently controlled, with each component having its own regulator. This control of the rotor currents makes it possible to generate the reference rotor voltages V_{rd_ref} and V_{rq_ref} to be applied to the pulse wide modulation (PWM) control stage of the converter [14]–[19]. The reference rotor current i_{rq_ref} and i_{rd_ref} are given respectively by (22) and (23) [14].

$$i_{rq\_ref} = -\frac{2}{3}\frac{L_s}{pL_m\psi_s}T_{em_{ref}} = -\frac{2}{3}\frac{L_s}{pL_m\phi_s}K_{opt}\omega_m^2 \tag{22}$$

$$i_{rd\_ref} = \frac{2}{3}(\frac{\phi_s}{L_m} - \frac{L_s}{V_sL_m})Q_{s\_ref} \tag{23}$$

The rotor current i_{rd} and i_{rq} are controlled by LADRC controllers as shown in Figure 5. These expressions can be rewriten using the canonical form given by (24) and (25).

$$\frac{di_{rd}}{dt} = -\frac{R_r}{\sigma L_r}i_{rd} + \omega_r i_{rq} + \frac{1}{\sigma L_r}v_{rd} \tag{24}$$

$$\frac{di_{rq}}{dt} = -\frac{R_r}{\sigma L_r}i_{rq} - \omega_r i_{rd} - \omega_r \frac{L_m}{\sigma L_s L_r}\phi_s + \frac{1}{\sigma L_r}v_{rq} \tag{25}$$
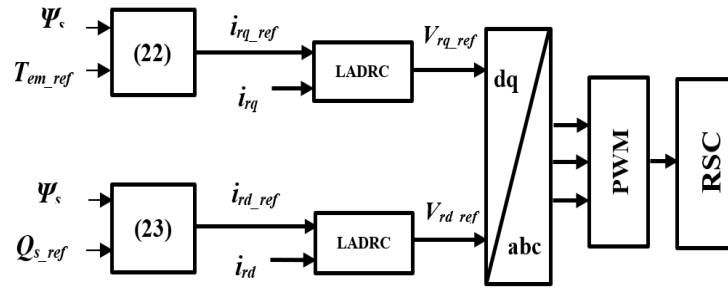
Figure 5. Control of the RSC using LADRC

The LADRC controllers are then designed by (26) and (28) as shown in.

$$\frac{di_{rd}}{dt} = f_d(\cdot) + b_{r0}u_d \tag{26}$$

Where:

$$\begin{cases} f_d(\cdot) = -\frac{R_r}{\sigma L_r}i_{rd} + \omega_r i_{rq} + (\frac{1}{\sigma L_r} - b_{r0})v_{rd} \\ b_{r0} = \frac{1}{\sigma L_r} \; ; \; u_d = v_{rd} \end{cases} \tag{27}$$

In addition:

$$\frac{di_{rq}}{dt} = f_q(\cdot) + b_{r0}u_q \tag{28}$$

Where:

$$\begin{cases} f_q(\cdot) = -\frac{R_r}{\sigma L_r}i_{rq} - \omega_r(i_{rd} + \frac{L_m\phi_s}{\sigma L_s L_r}) + (\frac{1}{\sigma L_r} - b_{r0})v_{rq} \\ b_{r0} = \frac{1}{\sigma L_r} \; ; \; u_q = v_{rq} \end{cases} \tag{29}$$

2.2.3. Linear active disturbance rejection control for grid side converter

The control block of the GSC is shown in Figure 6, which includes a direct current (DC) bus voltage control loop to keep it constant and a current control loop in the filter (R_f, L_f) which is used to generate reference V_{fd_ref} and V_{rq_ref} voltages which will be applied to the input of the PWM command of the converter [25], [26].

The filtre currents expression can be writen using the canonical form given by (30) and (31).

$$\frac{di_{fd}}{dt} = -\frac{R_f}{L_f}i_{fd} - \omega_s i_{fq} - \frac{1}{L_f}v_{fd} \tag{30}$$

$$\frac{di_{fq}}{dt} = -\frac{R_f}{L_f}i_{fq} + \frac{1}{L_f}V_s - \omega_s i_{fd} - \frac{1}{L_f}v_{fq} \tag{31}$$
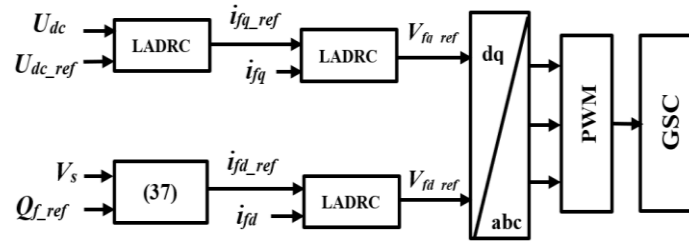
Figure 6. Control of the GSC using LADRC

Neglecting the losses in the filter (Rf, Lf), the active and reactive powers exchanged with the network are expressed by the (32) and (33).

$$P_f = \frac{3}{2}V_s i_{fq} \tag{32}$$

$$Q_f = \frac{3}{2}V_s i_{fd} \tag{33}$$

The power of the DC link capacitor C is described by (34).

$$P_{dc} = C U_{dc}\frac{dU_{dc}}{dt} \tag{34}$$

Where

$$\frac{dU_{dc}}{dt} = \frac{1}{C}(i_r - i_f) \tag{35}$$

The power on the DC bus is given by the (36).

$$P_{dc} = P_r - P_f \tag{36}$$

Where P_r, P_f are the generator rotor side and filter side powers respectively. The power sign P_r depends on how the generator works. P_r is positive in hyper-synchronous mode (the rotor provides power to the grid), and negative in hypo-synchronous mode (the rotor receives power from the grid). The reference current i_{fq_ref} comes from the internal voltage control loop of the DC bus voltage U_{dc}. To impose a zero reactive power on the grid, the reference current i_{fd_ref} can be given by (37).

$$i_{fd\_ref} = \frac{2}{3V_s}Q_{f\_ref} \tag{37}$$

The canonical forms of LADRC are given by (38) and (40).

$$\frac{di_{fd}}{dt} = f_{fd}(.) + b_{f0}u_{fd} \tag{38}$$

Where:

$$\begin{cases} f_{fd}(.) = \frac{R_f}{L_f}i_{fd} - \omega_s i_{fq} + \left(\frac{1}{L_f} - b_{f0}\right)V_{fd} \\ b_{f0} = -\frac{1}{L_f} \; ; \; u_{fd} = V_{fd} \end{cases} \tag{39}$$

In addition:

$$\frac{di_{fq}}{dt} = f_{fq}(.) + b_{f0}u_{fq} \tag{40}$$

Where:

$$\begin{cases} f_{fq}(.) = \frac{1}{L_f}V_s - \frac{R_f}{L_f}i_{fq} - \omega_s i_{fd} + \left(\frac{1}{L_f} - b_{f0}\right)V_{fq} \\ b_{f0} = -\frac{1}{L_f} \; ; \; u_{fq} = V_{fq} \end{cases} \tag{41}$$

3. RESULTS AND DISCUSSION

The WCS parameters used for the simulation are given in the Table 1 for the DFIG, Table 2 for the grid side and LADRC parameters. To justify the performance and robustness of the LADRC controller we tested and simulations of all parts of WCS, using the MATLAB/Simulink software. Two tests have been conducted under different conditions. In the first one the reference stator reactive power Q_{s_ref} has been set to zero and in the second one Q_{s_ref} has been set to $-1e^5 \, VAR$.

Table 1. The parameters of the DFIG

Parameters	Values
Rated power Pn	1.5 MW
Rated voltage Un	690 V
Nominal frequency	50 Hz
Rated rotor speed	1750 tr/min
Number of pole pairs	2
Rotor resistance Rr	2.65 mΩ
Stator resistance Rs	2.63 mΩ
Stator leakageinductance Lsσ	0.1687 mH
Rotor leakage inductance Lrσ	0.1337 mH

Table 2. Grid side and LADRC parametrers

Parameters	Values
Rated power	1.5 MW
Density of air	1.225 kg/m³
Blade radius	30
Gearbox ratio G	57
Kp	400
β01	2400
β02	1440000

3.1. Tracking test

In this test, as seen in the Figure 7, a variable speed wind profile is applied to the WT. Figure 8 illustrate the mechanical speed corresponding to the wind speed profile previously applied to the turbine. As seen in the Figure 9 the evolution of the power coefficient $Cp(\lambda,\beta)$ as a function of λ and for different values of β. It can be observed that when the pitch angle β increases, the coefficient Cp decreases, and which results in a reduction in the wind kinetic energy captured by the turbine. The maximum of power coefficient Cp is given for the pitch β fixed at 0. The Figure 10 presents the evolution of the power coefficient in the case of the pitch β equal to 0. The aim is to extract maximum power and to obtain a maximum power coefficient Cp.
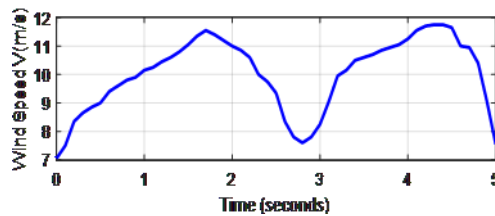
Figure 7. Wind speed profile
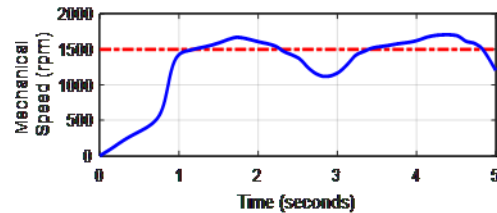
Figure 8. Mechanical speed (rpm)

The extracted mechanical power is shown in Figure 11. The Figures 12 and 13 illustrate respectively the evolution of the stator currents and rotor currents generated by the wind system. Figures 14 and 15 shows that the active power P_s and the reactive power Q_s at the stator level follow their references, proving that the control proposed by LADRC is robust and efficient. In Figure 16 the voltage Vdc of the DC bus is kept

constant with zero overshoot while Figure 17 represents the stator voltage Vsa and the stator current Isa. We can observe from Figure 17 that the voltage Vsa and the current Isa are in phase opposition which means that the DFIG operate in hyper synchronous mode.
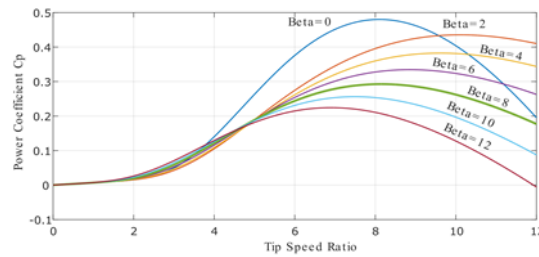
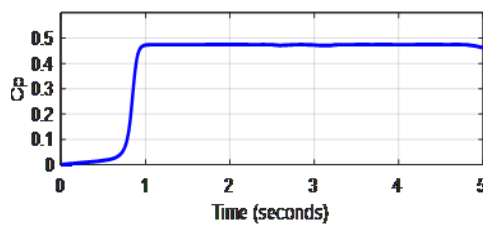Figure 9. Evolution of the Cp according to the speed ratio λ and the pitch angle β
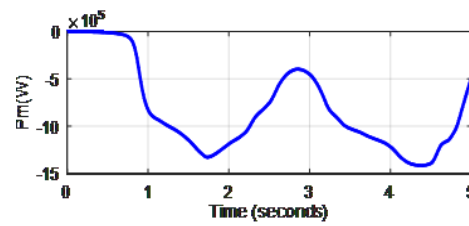

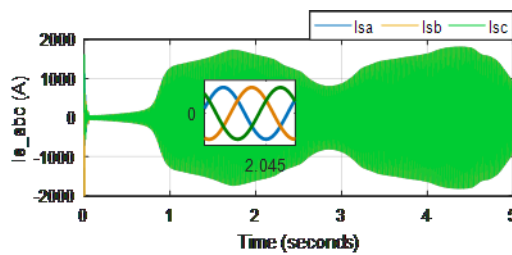Figure 10. Power coefficient Cp

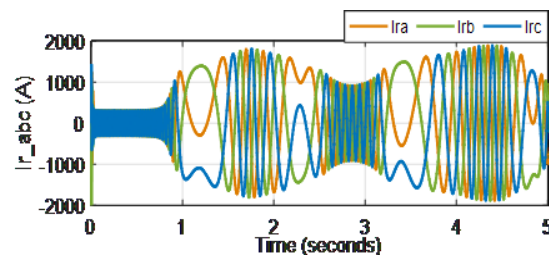

Figure 11. Mechanical power
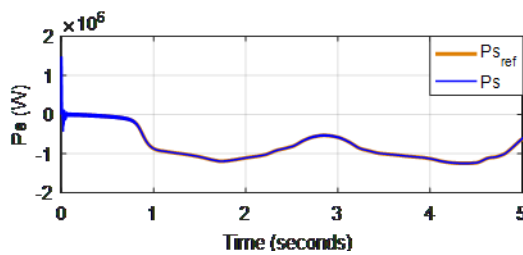

Figure 12. Stator currents

Figure 13. Rotor currents

Figure 14. Active stator power
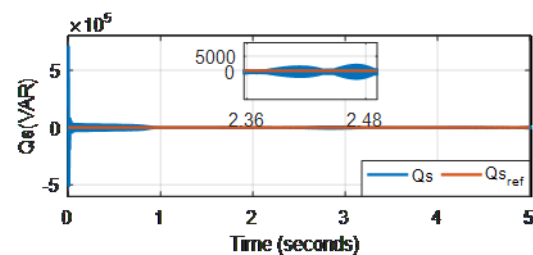
Figure 15. Reactive stator power
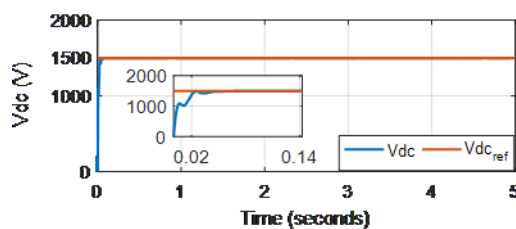
Figure 16. DC bus voltage
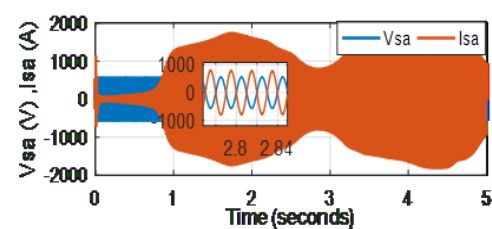
Figure 17. Stator voltage Vsa and stator current Isa

3.2. Comparison with backstepping controller

To prove the robustness of the LADRC controller, a comparative study with the backstepping controller was established. Figures 18 and 19 represent the results of the active and reactive powers injected into the grid by the rotor. Therefore, it can be concluded that the power factor is equal to unit since the reactive power has been set to zero. From the previous results, it can be said that the LADRC controller is fast, robust, and stable than the backstepping controller.
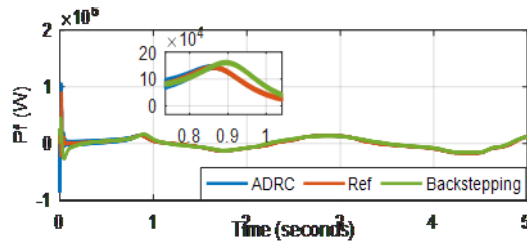
Figure 18. Active rotor power exchanged with the grid
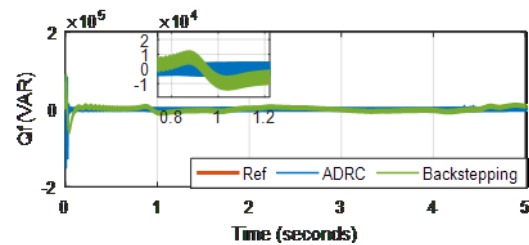
Figure 19. Reactive rotor power exchanged with the grid

3.3. Robustness test

The principle of this test consists in changing the internal DFIG model parameters, to test robustess of the proposed control against the effect of the dynamic behavior of the system. Figures 20(a) and 20(b) show the evolution of the active and reactive power injected by stator side. The same wind speed profile was applied tothe turbine and the reference reactive power is chosen as shown in: i) from t=0 to t=2.5 s and from t=4 s to t=5 s: Qs-ref=0 VAR, ii) from t=2.5 to t=4 s: Qs-ref=-1 e5VAR.

In this test, the rotor inductance Lr was changed by 20% and the resistance Rr was increased by 100%. One can clearly see in the Figure 20 that the variation of both resistance and inductance of the rotor has no effects when using LADRC control, which makes it possible to compensate the internal disturbances of the system. On the other hand and to demonstrate the performance of the LADRC regulator with respect to the backstepping controller, a comparison was made with a change of 35 % on the rotor inductance Lr. Figures 21 and 22 show that the LADRC controller is more stable and robust against model uncertainties that affect system stability.

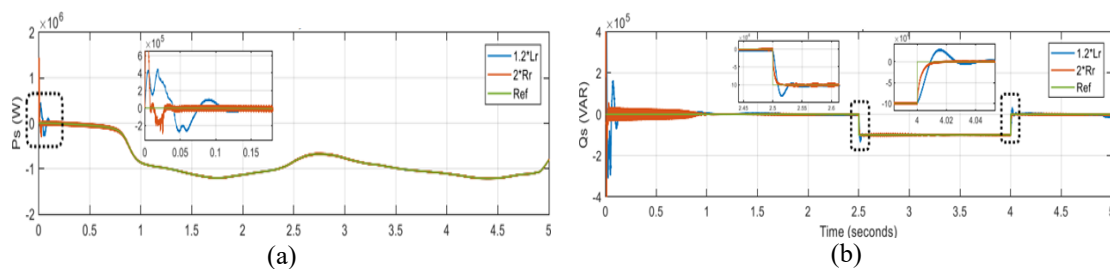(a)   (b)

Figure 20. Evolution of the (a) stator active power and (b) stator reactive power
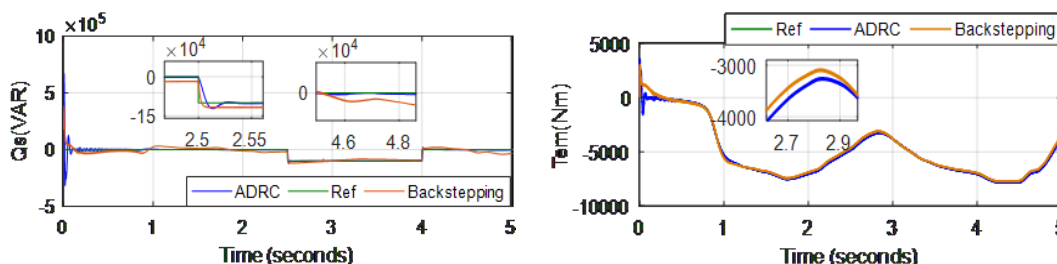

Figure 21. Stator reactive power of the DFIG for 35% Lr
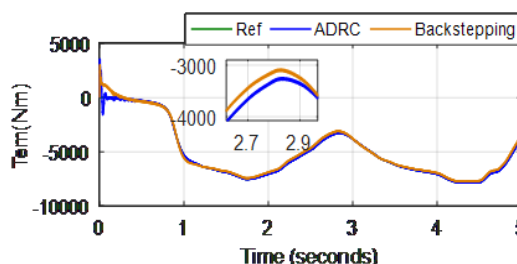
Figure 22. The electromagnetic torque of the DFIG for 35% Lr

4.   CONCLUSION

In this paper, a linear control strategy based on LADRC controllers was established to control the RSC, GSC, and DC bus voltage in order to extract the maximum power regardless of the speed of the wind applied to the turbine. A judicious choice of the gain and the parameters of the LESO used in the LADRC regulation loop made it possible, according to the simulation results on the MATLAB/SIMULINK software, to compensate all modeling errors and attenuate the impact of varying system parameters. To prove its robust foundation, a comparison with backstepping control has been drawn. The results obtained showed that the LADRC controller is more robust due to its ability to estimate and compensate internal and external disturbances affecting the system under study.

RERERENCES

[1]   H. Laghridat, A. Essadkil, M. Annoukoubil, and T. Nasser, "Linear Active Disturbance Rejection Control (LADRC) of a Variable Speed Wind Energy Conversion System using a DFI-Generator," *2018 6th International Renewable and Sustainable Energy Conference (IRSEC)*, 2018, pp. 1–6, doi: 10.1109/IRSEC.2018.8703027.

[2]   T. R. Ayodele, A. A. Jimoh, J. L. Munda, and J. T. Agee, "Challenges of grid integration of wind power on power system grid integrity: a review," *International journal of renewable energy research (IJRER)*, vol. 2, no. 4, pp. 618–626, 2012.

[3]   D. Chwa and K. Lee, "Variable Structure Control of the Active and Reactive Powers for a DFIG in Wind Turbines," in *IEEE Transactions on Industry Applications*, vol. 46, no. 6, pp. 2545–2555, November–December 2010, doi: 10.1109/TIA.2010.2073674.

[4]   Md. Arifujjaman, T. Iqbal, and J. E. Quaicoe, "Vector control of a dfig based wind turbine," *IU-Journal of Electrical & Electronics Engineering*, vol. 9, no. 2, pp. 1–9, January 2009.

[5]   Z. Rafiee, M. Rafiee, and M. Aghamohammadi, "A new control strategy based on reference values changing for enhancing LVRT capability of DFIG in wind farm," *International Journal of Renewable Energy Research (IJRER)*, vol. 9, no. 4, pp. 1626–1637, December 2019.

[6]   Y. Moumani, A. J. Laafou, and A. A. Madi, "Modeling and Backstepping Control of DFIG used in Wind Enegry Conversion System," *2021 7th International Conference on Optimization and Applications (ICOA)*, 2021, pp. 1–6, doi: 10.1109/ICOA51614.2021.9442625.

[7]   S. Bayhan, H. Abu-Rub, and O. Ellabban, "Sensorless model predictive control scheme of wind-driven doubly fed induction generator in dc microgrid," *IET Renewable Power Generation*, vol. 10, no. 4, pp. 514–521, 2016, doi: 10.1049/iet-rpg.2015.0347.

[8]   X. Liu, Y. Han, and C. Wang, "Second-order sliding mode control for power optimisation of DFIG-based variable speed wind turbine," *IET Renewable Power Generation*, vol. 11, no. 2, pp. 408–418, 2017, doi: 10.1049/iet-rpg.2015.0403.

[9]   M. I. Martinez, G. Tapia, A. Susperregui, and H. Camblong, "Sliding-Mode Control for DFIG Rotor- and Grid-Side Converters Under Unbalanced and Harmonically Distorted Grid Voltage," in *IEEE Transactions on Energy Conversion*, vol. 27, no. 2, pp. 328–339, June 2012, doi: 10.1109/TEC.2011.2181996.

[10]   G. S. Kaloi, J. Wang, and M. H. Baloch, "Dynamic Modeling and Control of DFIG for Wind Energy Conversion System Using Feedback Linearization," *Journal of Electrical Engineering and Technology*, vol. 11, no. 5, pp. 1137–1146, September 2016, doi: 10.5370/JEET.2016.11.5.1137.

[11]   F. Blaabjerg, M. Liserre, and K. Ma, "Power Electronics Converters for Wind Turbine Systems," in *IEEE Transactions on Industry Applications*, vol. 48, no. 2, pp. 708–719, March–April 2012, doi: 10.1109/TIA.2011.2181290.

[12]   J. Han, "From PID to Active Disturbance Rejection Control," in *IEEE Transactions on Industrial Electronics*, vol. 56, no. 3, pp. 900–906, March 2009, doi: 10.1109/TIE.2008.2011621.

[13]   M. Arbaoui, A. Essadki, I. Kharchouf and T. Nasser, "A New Robust Control by Active Disturbance Rejection Control Applied on Wind Turbine System Based on Doubly Fed Induction Generator DFIG," *2017 International Renewable and Sustainable Energy Conference (IRSEC)*, 2017, pp. 1-6, doi: 10.1109/IRSEC.2017.8477245.

[14]   A. J. Laafou, A. A. Madi, A. Addaim, and A. Intidam, "Dynamic Modeling and Improved Control of a Grid-Connected DFIG Used in Wind Energy Conversion Systems," *Mathematical Problems in Engineering*, vol. 2020, July 2020, doi: 10.1155/2020/1651648.

[15]   P. Maciejewski and G. Iwański, "Six-phase doubly fed induction machine-based standalone DC voltage generator," *Bulletin of the Polish Academy of Sciences. Technical Sciences*, vol. 69, no. 1, p. e135839, 2021, doi: 10.24425/bpasts.2021.135839.

[16]   R. Chakib, A. Essadki, and M. Cherkaoui, "Active Disturbance Rejection Control for Wind System Based On a DFIG," vol. 8, no. 8, pp. 1306–1315, 2014.

[17]   L. Djilali, E. N. Sanchez, and M. Belkheiri, "Real-time implementation of sliding-mode field-oriented control for a DFIG-based wind turbine," *International Transactions on Electrical Energy Systems*, vol. 28, no. 5, p. e2539, May 2018, doi: 10.1002/etep.2539.

[18]   A. J. Laafou, A. A. Madi, and A. Addaim, "Dynamic Control of DFIG used in Wind Power Production, based on PI regulator," *2020 IEEE 2nd International Conference on Electronics, Control, Optimization and Computer Science (ICECOCS)*, 2020, pp. 1–6, doi: 10.1109/ICECOCS50124.2020.9314563.

[19]   H. Laghridat, A. Essadki, M. Annoukoubi, and T. Nasser, "A Novel Adaptive Active Disturbance Rejection Control Strategy to Improve the Stability and Robustness for a Wind Turbine Using a Doubly Fed Induction Generator," *Journal of Electrical and Computer Engineering*, vol. 2020, March 2020, doi: 10.1155/2020/9847628.

[20]   M. Chakib, "A comparative study of PI, RST and ADRC control strategies of a doubly fed induction generator based wind energy conversion system," *International Journal of Renewable Energy Research (IJRER)*, vol. 8, no. 2, pp. 964–973, June 2018, doi: 10.20508/ijrer.v8i2.7645.g7383.

[21]   A. Jaballaafou, A. A. Madi, A. Addaim, and A. Intidam, "Wind Power Production based on DFIG: Modeling and Control by ADRC," *2020 IEEE 20th Mediterranean Electrotechnical Conference (MELECON)*, 2020, pp. 517–522, doi: 10.1109/MELECON48756.2020.9140611.

[22]   A. Boualouch, T. Nasser, A. Essadki, A. Boukhriss, and A. Frigui, "A robust power control of a DFIG used in wind turbine conversion system," *International Energy Journal*, vol. 17, no. 1, pp. 1–10, March 2017.

[23]   Z. Gao, "Scaling and bandwidth-parameterization based controller tuning," *Proceedings of the American control* conference, vol. 6, pp. 4989–4996, 2003, doi: 10.1109/ACC.2003.1242516.

[24] G. Herbst, "A Simulative Study on Active Disturbance Rejection Control (ADRC) as a Control Tool for Practitioners," *Electronics*, vol. 2, no. 3, pp. 246–279, September 2013, doi: 10.3390/electronics2030246.
[25] E. Chetouani, Y. Errami, A. Obbadi, and S. Sahnoun, "Optimal tuning of PI controllers using adaptive particle swarm optimization for doubly-fed induction generator connected to the grid during a voltage dip," *Bulletin of Electrical Engineering and Informatics*, vol. 10, no. 5, pp. 2367–2376, October 2021, doi: 10.11591/eei.v10i5.2843.
[26] I. Aboudrar, S. E. Hani, H. Mediouni, and A. Aghmadi, 'Active Disturbance Rejection Control of Shunt Active Power Filter Based on P-Q Theory', in *Recent Advances in Electrical and Information Technologies for Sustainable Development*, S. El Hani and M. Essaaidi, Eds. Cham: Springer International Publishing, 2019, pp. 173–182, doi: 10.1007/978-3-030-05276-8_19.

BIOGRAPHIES OF AUTHORS

Abdeslam Jabal Laafou 🆔 �8 ▨ Ⓟ was born in Morocco. He received Master degree of Electrical Engineering in 2014, from the ENSET of Rabat, Mohammed V University, Rabat, Morocco. He is currently a Ph.D student at National School of Applied Sciences, Ibn Tofail University, Kenitra Morocco. His research interests are control strategies of wind power systems. He can be contacted at e-mail: abdeslam.jaballaafou@uit.ac.ma.

Abdessalam Ait Madi 🆔 �8 ▨ Ⓟ �8 ▨ Ⓟ was born in Morocco. He received the teaching engineering degree in electronics from the ENSET of Mohammedia. He received the Master and Ph.D. degrees from the Faculty of Sciences and Technologies from the Sidi Mohamed Ben Abdellah University of Fez in Morocco. He received the Habilitation degree from the Faculty of Sciences of Ibn Tofail University. He is an Associate Professor at the National School of Applied Sciences of ibn Tofail University in Kenitra, Morocco. He can be contacted at email: abdessalam.aitmadi@uit.ac.ma.

Youssef Moumani 🆔 �8 ▨ Ⓟ received Master degree of Sciences and Technology speciality: Automatic, Signal Processing and industrial computing in 2014, from Faculty of Science and Technology, Hassan I University, Settat, Morocco. He is currently a PhD Student at National School of Applied Sciences, Ibn Tofail University, Kenitra Morocco. His research interests are control strategies of wind power systems. He can be contacted at e-mail: youssef.moumani@uit.ac.ma

Adnane Addaim 🆔 �8 ▨ Ⓟ he received his master diploma in 2001 and his Ph.D. degree in 2008, both in satellite communication from Mohammadia School of Engineers (EMI), Morocco. From 2002 to 2003, he was employed at SIEMENS.AG, as Engineer, responsible of the implementation of the supervision network of the Meditelecom GSM Network, in Morocco. From 2010 to 2020, he was a professor lecture at ENSA Engineering School at Kenitra, Morocco. Currently, he is a professor lecturer at the EMI Engineering School at Rabat, Morocco. His current research interests include signal processing, wireless communication networks and satellite communication systems. He can be contacted at e-mail: addaim@emi.ac.ma.